Aeolian Research 21 (2016) 45–52

Contents lists available at ScienceDirect

Aeolian Research

journal homepage: www.elsevier.com/locate/aeolia

3D numerical simulation of the evolutionary process of aeolian downsized crescent-shaped dunes

Xiaosi Zhou, Yang Zhang *, Yuan Wang, Min Li

Dept. of Fluid Machinery and Engineering, Xi'an Jiaotong University, Xianning Western Road 28, Xi'an 710049, China

ARTICLE INFO

Article history:
Received 14 January 2016
Accepted 1 March 2016
Available online 14 March 2016

Keywords:
Crescent-shaped dune
Downsized
Numerical stimulation
Modulation of gravity

ABSTRACT

A dune constitutive model was coupled with a large eddy simulation (LES) with the Smagorinsky subgrid-scale (SGS) model to accurately describe the evolutionary process of dunes from the macroscopic perspective of morphological dynamics. A 3D numerical simulation of the evolution of aeolian downsized crescent-shaped dunes was then performed. The evolution of the 3D structure of Gaussian-shaped dunes was simulated under the influence of gravity modulation, which was the same with the vertical oscillation of the sand bed to adjust the threshold of sand grain liftoff in wind tunnel experiments under the same wind speed. The influence of gravity modulation intensity on the characteristic scale parameter of the dune was discussed. Results indicated that the crescent shape of the dune was reproduced with the action of gravity during regulation of the saturation of wind-sand flow at specific times. The crescent shape was not dynamically maintained as time passed, and the dunes dwindled until they reached final decomposition because of wind erosion. The height of the dunes decreased over time, and the height–time curve converged as the intensity of modulation increased linearly. The results qualitatively agreed with those obtained from wind tunnel experiments.

1. Introduction

Barchans are crescent-shaped dunes formed under the actions of wind field with a single wind direction. Barchans attract widespread attention because of their unique structure, self-organising evolution and high-rate migration. Field observations indicate that migrating dunes of natural scale may take several months to several years to achieve total migration (Bagnold, 1941; Pye and Tsoar, 2009; Ewing et al., 2015). Downsized dunes are typically used to simulate dunes in real scale because of the finite size of a wind tunnel (Andreotti et al., 2002; Dauchot et al., 2002; Faria et al., 2011; Zhang et al., 2014). Dynamic numerical simulation is an alternative technique to field research to study dunes. This approach not only reveals the evolution of dunes at any scale but also enables the exploration of the influence of various factors on dune evolution under controllable conditions. Numerical simulation of the evolutionary process of dunes consumes reduced amount of time and is characterised by continuity, repeatability and independence from environmental factors. Therefore, numerical simulation provides great benefits as a supplement to wind tunnel simulation.

Simulation of the evolution and migration of dunes in a wind field poses greater challenges compared with simulation of near-surface wind-sand flow. The formation and migration of dunes are caused by interaction among three processes, namely, surface air flow movement, macroscopic surface changes and microscopic sand grain transport. The evolution and migration of dunes on the macroscopic scale are related to the characteristics of air and sand flow, as well as the erosion and deposition patterns of sand phase. Generally, dunes can be more comprehensively described by macroscopic parameters than by microscopic parameters. Studies have shown that the mesoscale aspects of sand flux are of greater significance than the characteristics of grains that constitute dunes in morphological research (Sauermann et al., 2001a; Hersen et al., 2002). Sauermann et al. (2001b) conducted field measurements of dunes and found that the content of grains that constitute an independent barchan reached an order of magnitude of about 10^{15} (one thousand trillions). Therefore, simulating discrete grain size is difficult in the field of dune morphology.

Numerous studies adopt the macroscopic scale to investigate the migration dynamics of dunes (Kok et al., 2012). Thus far, the proposed representative models include the continuous minimal model (Sauermann et al., 2001a,b; Kroy et al., 2002) and the discrete cellular automaton (CA) model (Werner, 1995). These two models have been constantly improved in subsequent studies

* Corresponding author.
E-mail address: zhangyang1899@mail.xjtu.edu.cn (Y. Zhang).

http://dx.doi.org/10.1016/j.aeolia.2016.03.001
1875-9637/

on models for dunes. The application of the continuous minimal model has been extended from 2D dunes to 3D dunes (Schwammle and Herrmann, 2005; Parteli et al., 2014a), from a single dune to multiple dunes (Duran et al., 2010) and even to dunes on Mars (Parteli et al., 2007). Katsuki et al. (2005) drew on the principle of the CA model and proposed a calculation model that considered saltation and avalanche. The dynamic process of migration and collision of aqueous barchans was reproduced by simulation. Narteau et al. (2009) proposed a lattice-gas cellular automaton model based on the CA model. Changes in the 3D morphology of dunes and shear stress on the dune surface in real space were simulated. The correlation between discrete and continuous simulation methods was established. This model was also used to study sand transport capacity and saturation mechanism (Gao et al., 2014). Bishop et al. (2002) improved the CA model through physical excitation. Discrete lattice dynamics method realistically simulated the formation and evolution of dune fields. As an available model with insights obtained from the minimal model (Parteli et al., 2014a), the CA model has been used to deepen our understanding of aeolian landscape development (Baas, 2013). Lima et al. (2002) proposed a model for the development of dune fields; in this model, barchans were treated as "interacting particles." The same kind of spatial correlations between dunes could be reproduced similar to that in real fields by using the rule of inter-dune sand flux for interaction among dunes. This type of model was subsequently extended to simulate the evolution of a transverse dune field. Field dunes with almost the same height and velocity were reproduced, and this process was not influenced by the initial configuration of the field and coalescence between dunes (Parteli and Herrmann, 2003). Zheng et al. (2009) proposed a comprehensive scale-coupled model of dune fields. The scale difference between grains and dunes was resolved by drawing on the concept of sand body element. The trans-scale simulation of the evolution of sand dune field was then established.

Changes in surface wind field in dune terrain differ from those in the entire dunes on the time scale (Sauermann et al., 2001b; Schwammle and Herrmann, 2004). These studies mostly focused on dynamic morphological changes in dunes and reproduction of dune evolution. Hence, simplification is necessary to correlate surface wind field with the morphological evolution of dunes. Surface shear stress in the continuous minimal model is also based on analytical approximation, rather than on solving real turbulent wind field (Sauermann et al., 2003); as such, separation of the structural evolution of dunes from instantaneous changes in the surface flow field of dunes and the simulation for each change do not conform to rapid changes in the dune structure because surface medium flows under laboratory conditions (wind tunnel or water channel experiments) (Andreotti et al., 2002; Hersen, 2005; Groh et al., 2008; Franklin and Charru, 2011). Moreover, barchans have a minimal length in the order of ten metres (Bagnold, 1941; Andreotti et al., 2002; Hersen et al., 2002); in this regard, dunes do not evolve into a stable barchan dune shape in air at the laboratory scale (Dauchot et al., 2002; Andreotti et al., 2002). Basing on these issues, Zhang et al. (2014) treated the upwind influx and the vertical oscillation effect of the sand bed, that is, gravity modulation, as potential modulating methods that affect dune evolution in the wind tunnel experiment. Both modulations exerted the same effect on regulating the saturation level of sand flux above the dune surface to reproduce the crescent-shaped dune configuration. In principle, an optimal numerical model can simulate the evolutionary process of dune at any scale. The present work only focuses on the evolution of 3D aeolian downsized dunes and compares it with actual cases in the corresponding experiments. Firstly, a large eddy simulation (LES) model is coupled to a constitutive equation of structural evolution of dunes to accurately simulate the complex turbulent wind flows over the dynamic dune surface and the associated changes in dune height at different positions. Following the idea of Zhang et al. (2014), an associated gravity modulation module is then introduced to investigate the influence of gravity modulation intensity on the spatial scale parameters of the dune. Simulation results are evaluated using wind tunnel experiment data, particularly at the evolutionary process of dune body at such scale. This study aims to deepen our understanding of the new mechanism to modulate the saturation level of sand flux during the evolutionary process of macroscopic dune configuration. Finally, the applicability of the proposed model and further developments are presented.

2. Mathematical model

2.1. Governing equations for wind flow

The turbulent flow in wind field at the near-surface atmospheric boundary layer is described by using incompressible LES equations. After spatial filtering, the following continuity and momentum equations for the resolved field are applied:

$$\frac{\partial \bar{u}_{g,i}}{\partial x_i} = 0 \tag{1}$$

$$\frac{\partial}{\partial t}(\bar{u}_{g,i}) + \bar{u}_{g,j}\frac{\partial}{\partial x_j}(\bar{u}_{g,i}) = -\frac{1}{\rho_g}\frac{\partial \bar{p}_g}{\partial x_i} + \nu_{gl}\frac{\partial^2 \bar{u}_{g,i}}{\partial x_j \partial x_j} - \frac{1}{\rho_g}\frac{\partial \tau_{ij}}{\partial x_j} \tag{2}$$

where superscript "–" represents the spatially filtered variable, ν_{gl} is the kinematic viscosity of air and τ_{ij} is the subgrid-scale stress. Based on the Boussinesq hypothesis,

$$\tau_{ij} = -2\mu_{gt}\bar{S}_{g,ij} + \frac{1}{3}\tau_{kk}\delta_{ij} \tag{3}$$

where τ_{kk} is the isotropic part of the subgrid-scale stress, which is not modelled but added to the filtered static pressure term; δ_{ij} is the Kronecker delta; $\bar{S}_{g,ij} = \frac{1}{2}\left(\frac{\partial \bar{u}_{g,i}}{\partial x_j} + \frac{\partial \bar{u}_{g,j}}{\partial x_i}\right)$ is the rate of strain tensor of the resolved flow; and μ_{gt} is the eddy viscosity. Based on the model of Smagorinsky (1963), eddy viscosity is modelled by

$$\mu_{gt} = \rho_g (C_g \Delta)^2 |\bar{S}| \tag{4}$$

$$\bar{S} = \sqrt{2\bar{S}_{g,ij}\bar{S}_{g,ij}} \tag{5}$$

where C_g is the Smagorinsky constant, with a value of 0.1; and $\Delta = (\Delta x \Delta y \Delta z)^{1/3}$ is the filtered width.

2.2. Constitutive equations for dune evolution

The following equation represents the mass conservation of dune:

$$\rho_s \frac{\partial}{\partial t}(h) + \nabla \cdot q = 0 \tag{6}$$

where ρ_s, $h = h(x,z,t)$, and $q = q(x,z,t)$ are the apparent density of sand phase, dune height and total vertically integrated sand flux, respectively; $\rho_s = \rho_m(1-\lambda)$, where ρ_m is the density of sand grains, with value set as $\rho_m = 2650\ \mathrm{kg \cdot m^{-3}}$; and λ is the sand porosity. Total vertically integrated sand flux is divided into three parts: saltation, reptation and creep fluxes. The use of Sorensen's empirical formula (Sorensen, 1991) for saturated saltation flux exhibits good agreement with the wind tunnel experiments (Sauermann et al., 2003)

$$q_{sat} = \begin{cases} C_{sat}\frac{\rho_g}{g}u_*(u_* + 7.6u_t + 2.05), & u_* > u_t \\ 0, & u_* \leqslant u_t \end{cases} \tag{7}$$

where C_{sat} is the model coefficient; g is the gravity acceleration constant; and u_* and u_t are the friction and critical friction velocities, respectively. The expression of critical friction velocity considering the slope effect is as follows (Iversen and Rasmussen, 1994):

$$u_t = \Theta\sqrt{(\rho_m - \rho_g)gd_s(\cos\theta_s + \sin\theta_s/\tan\theta_{\text{rep}})/\rho_g} \tag{8}$$

where the coefficient Θ is 0.1 (Bagnold, 1941); d_s is the average grain size; θ_s is the slope angle; $\tan\theta_s = \nabla h$; and θ_{rep} is the angle of repose, $\theta_{\text{rep}} \approx 32^\circ$ (Iversen and Rasmussen, 1994).

Considering the transition of saltation flux from non-saturation to saturation (Hersen, 2004), then

$$\nabla \cdot q_{\text{sal}} = (q_{\text{sat}} - q_{\text{sal}})/l_{\text{sat}} \tag{9}$$

where q_{sal} is the saltation flux; and l_{sat} is the saturation length, which is the length scale for measuring whether q_{sal} reaches q_{sat}. In accordance with the case in which grain inertia is the dominant mechanism of transport rate saturation, the saturation length is proportional to the drag length of sand grain (Sauermann et al., 2001a) and slightly depends on the friction velocity (Pahtz et al., 2014).

$$l_{\text{sat}} = al_{\text{drag}} = a\rho_m d_s/\rho_g \tag{10}$$

where a is the proportional factor with a value of 20 after considering field and laboratory measurements (Bagnold, 1941; Hersen et al., 2002); and l_{drag} is the drag length of sand grain and represents the distance through which the sand grain reaches the wind speed from standing at a site on the surface.

Studies show that reptation induced by sand grain saltation considerably affects the transverse deposition of dune (Andreotti et al., 2002; Hersen, 2004). Reptation flux should be considered in describing dune shaping and evolution. On the basis of the relationship between saltation and reptation, the following expression is used to represent reptation flux (Andreotti et al., 2002; Andreotti, 2004):

$$q_{\text{rep}} = C_{\text{rep}}\sqrt{gd_s}q_{\text{sal}}/u_* \tag{11}$$

Creep also influences dune shaping. The relevant model derived by Wang and Zheng (2004) is considered to correlate creep flux with friction velocity:

$$q_{\text{cre}} = \frac{2\rho_g C_0^2}{\rho_m g^2 C_1}\left[(1+v_0)\ln\frac{(1+v_0)v_{\max}}{(1+v_{\max})v_0} - \frac{(v_{\max}-v_0)}{v_{\max}}\right]u_*^2 \tag{12}$$

where C_0 and C_1 are model constants; and v_0 and $v_{\max}$ are volume fraction and maximum volume fraction of sand, respectively. The value of $v_{\max}$ is set as 0.75 by simplifying sand grains into regular spherical grains.

Avalanche phenomenon on the barchan surface during evolution can be explained by the slope angle θ_s, which exceeds the angle of repose θ_{rep}. Instantaneous slippage occurs under the action of gravity, and sands are reallocated to different positions of the dune. Avalanche is a mechanism that drives the evolution of dunes and should be described using a specific model. The avalanche flux related to dune height (Duran et al., 2010) is converted into the concept of diffusion flux proposed by Ortiz and Smolarkiewicz (2006) to introduce a diffusion term in the dune evolution equation:

$$q_{\text{ava}} = -\rho_s\kappa\nabla h \tag{13}$$

where κ is the diffusion coefficient, which depends on the time step and the grid spacing of the simulation. When $\theta_s \leqslant \theta_{\text{rep}}$, no avalanche or slippage will occur. At this time, $q_{ava} = 0$. Thus,

$$\kappa = \begin{cases} -E\left[\tanh(|\nabla h|) - (\tan\theta_{\text{rep}})\right]/(|\nabla h|\rho_s), & |\nabla h| > \tan\theta_{\text{rep}} \\ 0, & |\nabla h| \leqslant \tan\theta_{\text{rep}} \end{cases} \tag{14}$$

where E is the empirical model parameter. The empirical value is set as -0.9 to ensure the stability of the calculation.

Changes in the sum of q_{sal}, q_{rep} and q_{cre} are equivalent to alterations in the average velocity of dune in the horizontal direction u_m and in the dune height h. The total vertically integrated sand flux is obtained by considering the avalanche flux.

$$q = \rho_s(u_m h - \kappa\nabla h) \tag{15}$$

After substituting Eq. (15) into Eq. (6), the mass conservation equation of dune used for discretisation is obtained.

$$\frac{\partial}{\partial t}(h) + \nabla \cdot u_m h = \nabla \cdot \kappa\nabla h \tag{16}$$

2.3. Numerical method

SIMPLE algorithm (Patankar, 1980) based on finite control volume technique is used to couple gas phase velocity field and pressure field. Eq. (16) is a continuous equation for dune height and has a similar form to the momentum equation for the gas phase. The transient, convective and diffusion terms are shown from left to right of the equation. Therefore, discretizing scheme is adopted for the corresponding terms in the equations for gas phase and dune. The stability-guaranteed second-order difference scheme is employed for spatial discretisation of convective term (Li and Tao, 2002); the second-order central difference scheme is utilised for diffusion term; and the fully implicit scheme is used for the transient term. The numerical process is as follows. (1) Gas phase field is calculated iteratively using the time step Δt_u. (2) After iteration for two time steps, the evolution of the dune is calculated iteratively using the time step in equation for dune Δt_h. (3) After obtaining the dune height $h(x,z,t)$ at different positions at this point in time, the iterative steps before the iteration of gas phase field are repeated, and a new distribution of heights of dune $h(x,z,t+\Delta t_h)$ is obtained. (4) These steps are repeated until the entire structural evolution process of the dune is simulated.

3. Coordinate conversion and simulation conditions

3.1. Coordinate conversion

The equation under the physical coordinate system (x,y,z,t) must be converted under the calculation coordinate system (ξ,η,ζ,τ) to conduct discretisation. The following treatment is adopted based on the actual physical process of the evolution of dunes (Wedi and Smolarkiewicz, 2003): $x = \xi$, $z = \zeta$, $t = \tau$ and $\eta = L_y(y-h)/(L_y-h)$. Thus, the Jacobian determinant for the transformation of governing equations is obtained. J can be expressed as $J = \left(\frac{\partial\xi}{\partial x}\frac{\partial\eta}{\partial y}\frac{\partial\zeta}{\partial z}\right)^{-1} = \left(\frac{\partial\eta}{\partial y}\right)^{-1} = (L_\eta - h)/L_\eta$. An analogy is inferred with the general conversion of coordinates by combining the Jacobian determinant J and the terms that involve the geometry of the grid, namely, $\partial\xi/\partial x$, $\partial\eta/\partial y$ and $\partial\zeta/\partial z$. The specific implementation process is shown in the work of Anderson (1995). The size of the calculation domain in stream-wise, vertical and span-wise directions is $L_\xi \times L_\eta \times L_\zeta = 7.225\ \text{m} \times 2.131\ \text{m} \times 3.825\ \text{m}$; and the grid number is $N_\xi \times N_\eta \times N_\zeta = 72 \times 42 \times 39$. The equation is discretised using the staggered grid system. The calculation domain and staggered grid system are shown in Fig. 1(a).

3.2. Simulation conditions

3.2.1. Boundary conditions

Wind flows from the inlet to the outlet of the calculation domain. Periodic boundary conditions are set for stream-wise

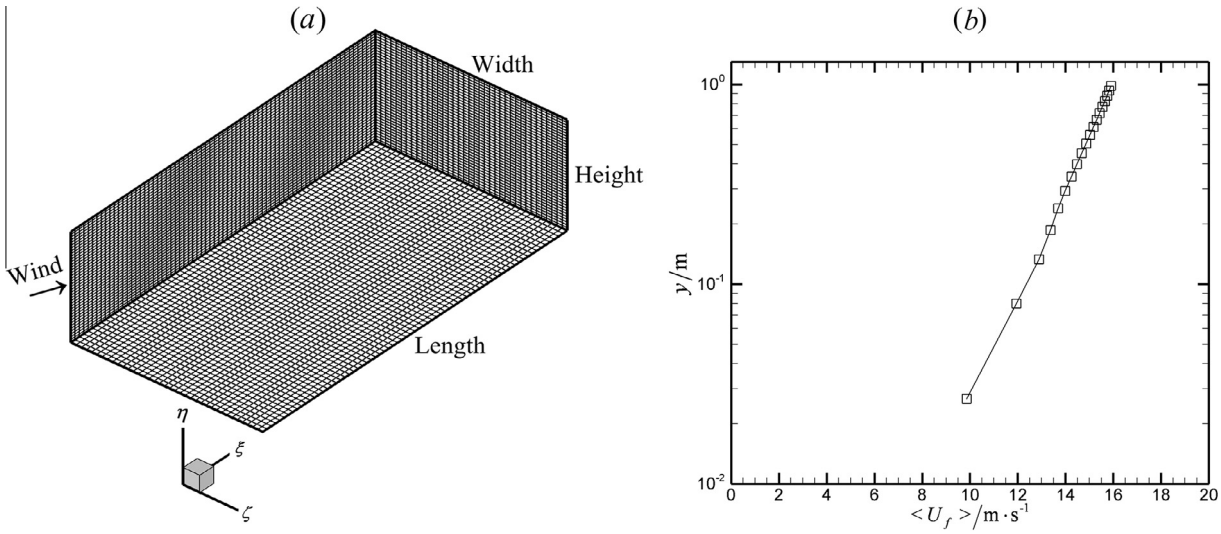

Fig. 1. Calculation domain and its inlet stream-wise wind speed: (a) grid system; and (b) simulated wind speed profile.

and span-wise directions of the calculation domain. Symmetrical boundary conditions are set at the top interface in the vertical direction. The vertical component of wind speed is set to zero at the top interface. The gradients of other variables of the flow field along the vertical direction are set to zero. The bottom interface is the wall boundary layer (including the dune surface). No slip is set for the wind field at the bottom interface. A semi-empirical formula is adopted as wall functions based on the work of Werner and Wengle (1991) to model the near-wall region of the high Reynolds turbulent wind flow field because of the large eddy simulation in the computational fluid dynamics framework. After the wall shear stress in the near-wall control volume τ_w is calculated by the Werner–Wengle wall functions, the friction velocity u_*, which is used to calculate sand flux on the dune surface, is obtained by $u_* = \sqrt{\tau_w/\rho_g}$.

3.2.2. Initial conditions

The flow field is initialised with respect to the logarithmic profile of the wind speed, that is, $u(x,y,z) = u_*/k \cdot \ln(y/y_0)$, where u_* is the friction velocity; $k = 0.41$ is the von Kármán constant; and y_0 is the surface roughness and $y_0 = d_s/30$. The average velocity profiles are superimposed by adopting the Gaussian distributed pulsating quantity of random velocity with zero mean and 5% of the wind speed of the main flow as variance at initial time. Therefore, the transition occurs from the laminar flow to the turbulent flow. The initial intensity of the wind field pressure is set to zero. The ambient temperature of the wind field during the simulation is maintained at 15 °C, and the physical parameters of simulation are determined under this condition. The wind speed profiles are calculated as shown in Fig. 1(b). The symbol $\langle\cdot\rangle$ denotes the operation of the ensemble average. Here, $\langle U_f\rangle$ is the ensemble-averaged stream-wise wind speed at the inlet of the calculation domain; hence, the inlet stream-wise wind speed is averaged spatially along the span-wise direction of the calculation domain at each step and then averaged temporally over the entire statistical time step. The wind speed of the main flow $U_0 = 14.5\ \mathrm{m \cdot s^{-1}}$, and the friction velocity is $0.608\ \mathrm{m \cdot s^{-1}}$. The initial values of the vertical component v and span-wise component w of wind speed are set to zero.

The following Gaussian function is used to simulate a single initial dune: $h = h_0 \exp[-(2r/r_0)^2 \cdot \ln 2]$, where h_0 and r_0 are the height of the highest point on the surface of the dune and the radius of the bottom of the dune, respectively; and r is the position function, that is, $r = [(x - x_0)^2 + (z - z_0)^2]^{1/2}$, where x_0 and z_0 are the coordinates of the central point at the bottom of the dune in the stream-wise and span-wise directions, respectively. The initial structure and position of the dune in the physical domain are shown in Fig. 2.

3.2.3. Simulation conditions

The simulation parameters are set as follows: average grain diameter, $d_s = 250\ \mu\mathrm{m}$; sand porosity, $\lambda = 0.38$; air density, $\rho_g = 1.225\ \mathrm{kg \cdot m^{-3}}$; and dynamic viscosity of air, $\mu_{gl} = 1.8 \times 10^{-5}\mathrm{kg \cdot m^{-1} \cdot s^{-1}}$. The Courant–Friedrichs–Lewy (CFL) condition is considered to determine the limited range of time step. The maximum Courant number can be estimated as follows (Koutsourakis et al., 2012): $\mathrm{CFL_{max}} = \Delta t \max\left(\frac{|u|}{\Delta x} + \frac{|v|}{\Delta y} + \frac{|w|}{\Delta z}\right) \leqslant 0.3$. In this case, the time step is less than or equal to 2.0×10^{-3} s. The iteration time step value should be reduced at least in the order of one for the wind flow equation to obtain high precision of the large eddy simulation. Therefore, in the present simulation, the time step for the equation for wind is $\Delta t_u = 2.0 \times 10^{-4}$ s, and time step for the equation for dunes is $\Delta t_h = 2.0 \times 10^{-3}$ s. As shown in Fig. 3, based on the fact that the threshold of grain liftoff in sand motions can be adjusted through oscillation, a vertically oscillating plate used to hold the sand bed and the dune were introduced in the wind tunnel experiment of Zhang et al. (2014). The instantaneous acceleration of gravity of individual grain can change over time because of the effect of plate oscillation. In this case, the initiation and the amount of sand grains for splash can be regulated to influence the evolution of dunes. This modulation approach is called "gravity modulation" (Fig. 3(b)). In the present model, changes in dune height in every grid cell position on the $x - z(\xi - \zeta)$ surface are used to show the variation in dune surface with time. This morphological process is related to the mesoscale aspects of sand flux, and the tracking of the movement of individual sand grains on dune surface is infeasible. Considering this narrow limitation, the upwind influx, as one modulation similar to the natural evolution of barchans, cannot be realised. The same form of gravity modulation used in the wind tunnel experiment (Zhang et al., 2014) is used in the present simulation because upwind influx and gravity modulation are comparable (Zhang et al., 2014). The oscillation of the bed surface is simulated using the cosine function of gravity acceleration, which changes over time. The threshold for sand

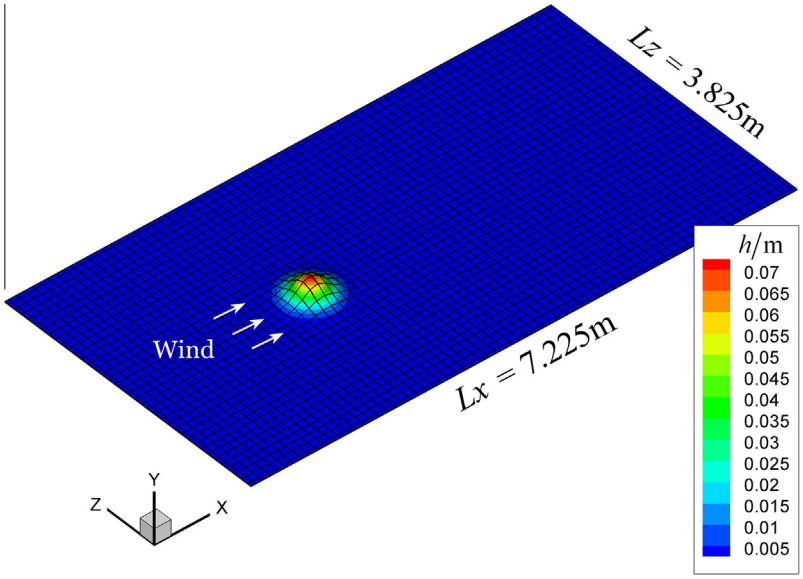

Fig. 2. Initial structure and position of dune in the physical domain.

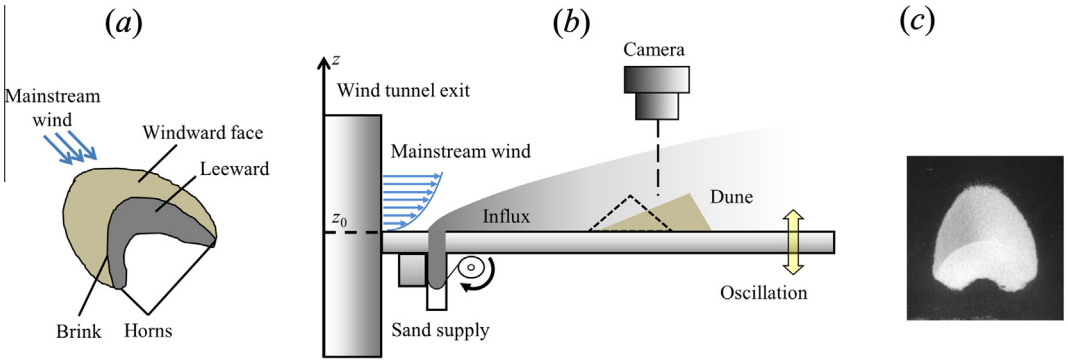

Fig. 3. Wind tunnel experiment of Zhang et al. (2014): (a) sketch of a crescent-shaped dune; (b) experimental setup; and (c) original image of downsized crescent-shaped dune.

grains to start oscillation is changed through gravity modulation. Therefore, the saturation of wind-sand flow can be regulated. The influence of modulation of gravity on the evolution of downsized crescent-shaped dunes is also discussed. The cosine function of gravity modulation is expressed as $g(T) = g_0 + 4\pi^2 M \cos(20\pi T)$, where $g_0 = 9.81\ \mathrm{m \cdot s^{-2}}$; M is the modulation factor with values of 0.2, 0.4, 0.6 and 0.8, which correspond to four simulation conditions. This function can be used to characterise the intensity of gravity modulation. The initial height of the dune is 0.075 m, and the radius of its bottom is 0.390 m.

The dimensionless similarity criterion is determined based on simulation parameters. In the simulations, the wind speed of the main flow U_0 and the initial height of the dune h_0 are set as two characteristic parameters, which correspond to Reynolds number $\mathrm{Re} = U_0 h_0 \rho_g / \mu_{gl} = 7.40 \times 10^4$ and Froude number $\mathrm{Fr} = U_0 / \sqrt{h_0 g_0} = 16.90$.

4. Results and discussion

4.1. Grid refinement study

A grid refinement study or a grid independence test is required to determine the proper grid size in the present study. Grid independence test is used to study the sensitivity of the numerical solution to the size of the grid and then decide the value of grid number to be used for the simulations. A grid independence test is performed by systematically increasing the number of grid nodes and comparing the results. After comprehensively considering the convergence, precision, and efficiency of the simulation, three grid systems are adopted: $62 \times 32 \times 29$, $72 \times 42 \times 39$ and $82 \times 52 \times 49$, which correspond to the coarse, medium and fine grid sizes, respectively. Fig. 4 shows the result of the comparison. As shown in Fig. 4, T_u is the predicted turbulence intensity of free stream wind flow $T_u = (< u_g'^2 >)^{1/2}/U_0$, where u_g' is the stream-wise component of instantaneous fluctuating velocity of wind. After a grid system of $72 \times 42 \times 39$, the profile of T_u does not significantly change with grid size. Therefore, using the grid number $N_\xi \times N_\eta \times N_\zeta = 72 \times 42 \times 39$ for the present simulation is appropriate.

4.2. Evolution pattern of a single dune

The evolution of a single downsized dune under the condition of $M = 0.8$ over time is shown in Fig. 5. The distribution of instantaneous wind field speed on the dune surface at different time points under the condition of $M = 0.8$ is shown in Fig. 6. Fig. 5 shows that the dune dwindles and finally decomposes over time because of the erosion of windward face, deposition, avalanche and low-rate

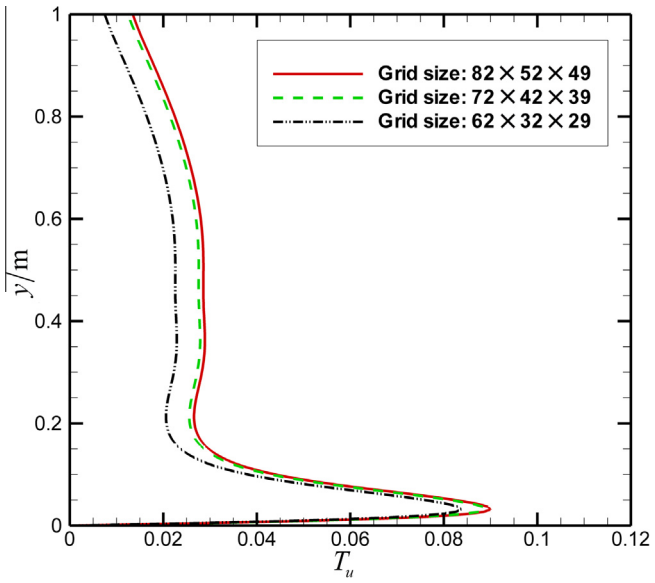

Fig. 4. Result of grid independence test.

backflow at the leeside (Fig. 6). At a certain time point during the evolution, the sand body takes a crescent shape, which cannot be maintained dynamically. Similar rules of evolution are observed under other simulation conditions. These unstable dune evolution processes are also observed in the experiment of Zhang et al. (2014) under the same gravity modulation and in the experiment of Andreotti et al. (2002) under the upwind influx effect. Fig. 5 shows that, with the middle point of the dune as the datum, the dune in the span-wise direction is not strictly symmetrical. This feature, which occurs during the reconstruction of the dune surface, is also observed in the wind tunnel experiment and water channel experiment for downsized barchans under the unidirectional medium flow condition (Andreotti et al., 2002; Franklin and Charru, 2011). Field studies (Bourke, 2010) and model simulations (Parteli et al., 2014a) on barchan asymmetry show that asymmetry is caused by four potential mechanisms, namely, bi-directional winds, dune collision, topography and influx asymmetry. However, in the present simulation, only the evolution process of an isolated downsized dune on the flat bed under the actions of wind field with a single wind direction is investigated. This process is simplified compared with the real dune fields. Therefore, the potential causes for existing slight asymmetry are unlikely to be bi-directional winds, dune collision and topography. As upwind influx is not used to influence dune evolution in the simulations, influx asymmetry does not influence dune asymmetry. The slight asymmetry of crescent-shaped dune body could be attributed to several factors. Firstly, in the simulations, periodic boundary conditions are set for stream-wise and span-wise directions of the calculation domain to ensure mass conservation for wind field and dunes. Therefore, the downstream turbulent flow from the leeside of the dune may disturb the upwind flow during dune evolution. In this case, the dune body may become asymmetric. This finding may explain why the upstream distribution of instantaneous turbulent wind field speed on the dune surface at a certain time point displays an asymmetric pattern (Fig. 6). Furthermore, although the crescent shape of downsized dune is reproduced with the action of gravity modulation, the crescent shape cannot be maintained dynamically all the time. Under the influence of wind erosion at the windward side combined with the complex recirculating flow structures at the lee side, the dune body gradually shrinks. These phenomena may contribute to the asymmetrical propagation of the two limbs of crescent-shaped dune.

4.3. Influence of gravity modulation intensity on structural parameters of dunes

Changes in dune height under different gravity modulation intensities over time are shown in Fig. 7(a). All of the simulated curves are the results of secondary polynomial fitting. The data of the wind tunnel experiment (Zhang et al., 2014) in the figure are the results of nondimensionalisation of the square root of the project area in the top view, which also reflect changes in dune height under erosion. Nondimensionalisation is performed using the following equation to facilitate the comparison of results:

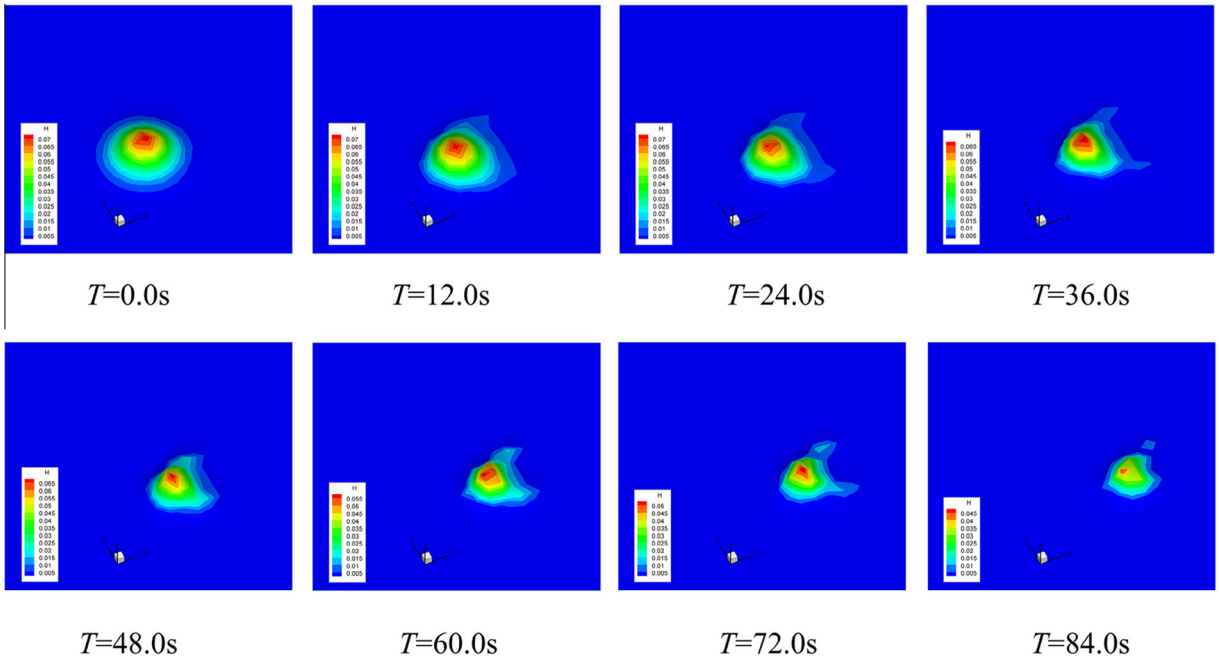

Fig. 5. Evolution of dune (M = 0.8).

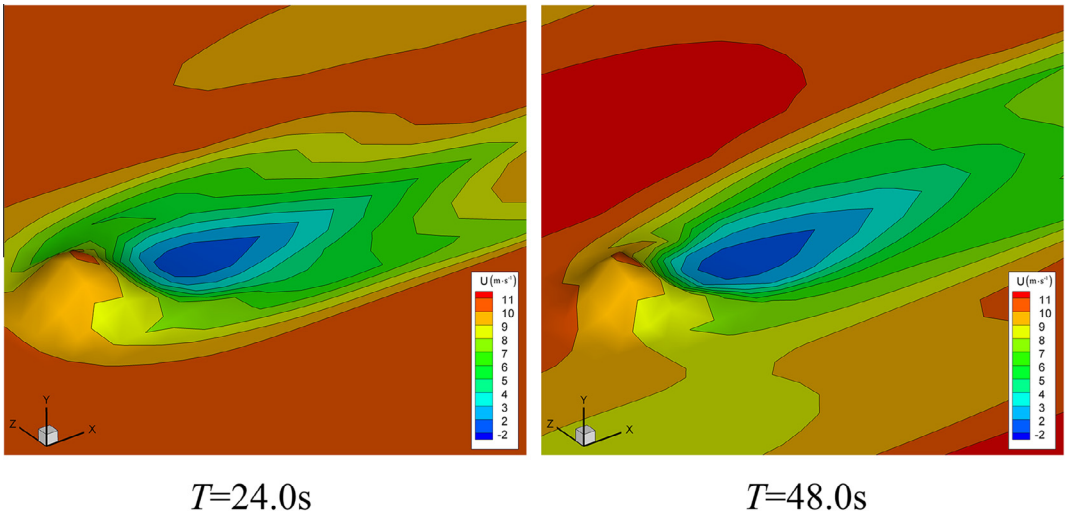

Fig. 6. Low-speed flow region at the leeward face of crescent-shaped dune at a certain time point during evolution (M = 0.8).

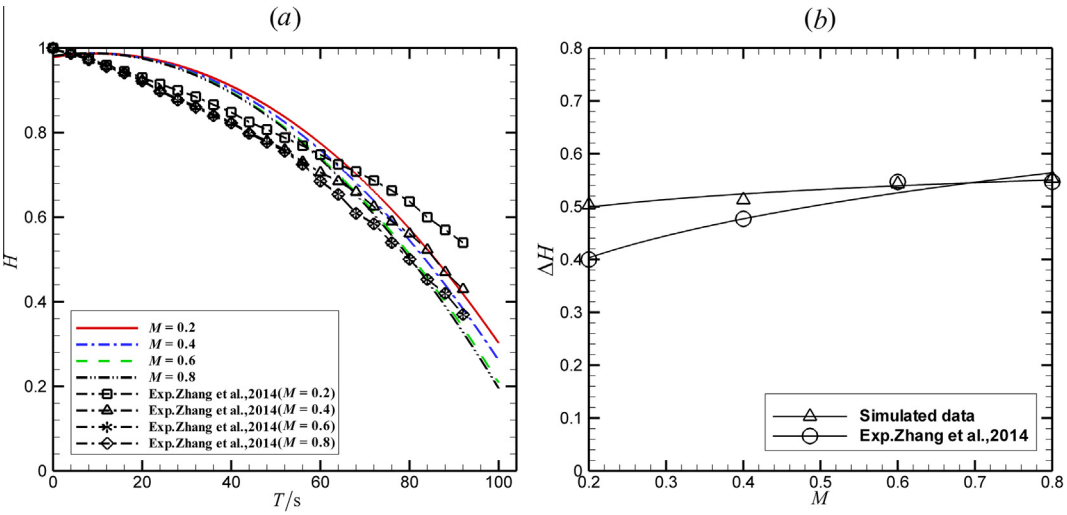

Fig. 7. Influence gravity modulation intensity on dune height: (a) variation in H with time; and (b) scope of variation of H with linear increase in gravity modulation intensity.

$H = h_{max}(T)/h_0$, where $h_{max}(T)$ is the height of the highest point on the dune surface at the time point T. The scope of variation of H under different intensities of gravity modulation is shown in Fig. 7(b). Here, ΔH denotes the range of H for a single $H-T$ relationship at $T = 90.0$ s. Both the simulated data and the corresponding experimental data curves are the results of secondary polynomial fitting. Fig. 7(a) shows that H finally decreases with increasing T under a fixed value of M. Therefore, the wind-sand flow on the dune surface is not yet saturated during erosion. As M increases linearly, the curve of $H-T$ gradually converges (Fig. 7(b)). Thus, as M increases, the wind-sand flow reaches saturation gradually. The results are consistent with those from wind tunnel experiments (Zhang et al., 2014). Changes in gravity modulation intensity in the wind tunnel experiments can alter saltation flux, thereby regulating the saturation state. However, the movement of discrete sand grains is not simulated in the present dune model. Therefore, changes in gravity alter the sand flux in the constitutive equation and regulate the saturation. This comparison indicates that the simulation and the experiment achieved consistent results with regard to the regulatory effect of gravity modulation on the saturation of wind-sand flow.

The combination of Fig. 7(a) and (b) shows that the coincidence between the simulation result and the experimental data increases with increasing gravity modulation intensity. The finding also indicates that high gravity modulation intensity result in the saturation of wind-sand flow.

5. Conclusion

In this study, large eddy simulation was coupled with a dune constitutive model. This approach was used in the 3D numerical simulation for the entire aeolian flow field to investigate the evolutionary characteristics of downsized crescent-shaped dunes under the influence of gravity modulation. Results show that the proposed model can reproduce a crescent shape, which is not strictly symmetrical. The unstable evolution rule of dune from the simulation agrees with that from the corresponding wind tunnel experiments. Dune height decreased over time, and the height–time curve gradually converged with the linear increase in gravity modulation; this finding agrees approximately with the result of the wind tunnel experiment. Hence, the gravity modulation mechanism embedded in the present model potentially

affects the regulation of the saturation level of sand flux above the dune surface, thereby considerably producing the macroscopic crescent-shaped dune configuration at the laboratory scale.

The simulation outcome agrees with the experimental results, thereby indicating that the proposed modelling approach could facilitate the study of the morphodynamic process of aeolian dunes at the laboratory scale and their comparison with natural cases. Furthermore, this model combined with the computational fluid dynamics framework to investigate the interaction dynamics of two or more barchans in depth is feasible because it can reveal reverse flow at the lee. Finally, morphodynamic modelling of aeolian dunes (Parteli et al., 2014b) has provided insights for developing application models for determining the effect of biogenic crust or space module of fences on dune morphology. This model is a potential tool to deepen understanding of the physical processes and fundamental principles in preventing soil erosion.

Acknowledgement

The authors gratefully acknowledge the support provided by the Natural Science Foundation of China (11402190, 11272252) and the China Postdoctoral Science Foundation (2014M552443).

References

Anderson, J.D., 1995. Computational Fluid Dynamics: The Basics With Applications. McGraw-Hill, New York.
Andreotti, B., 2004. A two species model of aeolian sand transport. J. Fluid Mech. 510, 47–70.
Andreotti, B., Claudin, P., Douady, S., 2002. Selection of dune shapes and velocities. Part 1: dynamics of sand, wind and barchans. Eur. Phys. J. B 28, 321–339.
Baas, A.C.W., 2013. Modeling aeolian landscapes. In: Shroder, J.F. (Ed.), Treatise on Geomorphology, 11. Academic Press, San Diego, pp. 313–327.
Bagnold, R.A., 1941. The Physics of Blown Sand and Desert Dunes. Methuen, London.
Bishop, S.R., Momiji, H., Carretero-Gonzalez, R., Warren, A., 2002. Modeling desert dune fields based on discrete dynamics. Discrete Dyn. Nat. Soc. 7, 7–17.
Bourke, M.C., 2010. Barchan dune asymmetry: observations from Mars and Earth. Icarus 205, 183–197.
Dauchot, O., Lechenault, F., Gasquet, C., Daviaud, F., 2002. "Barchan" dunes in the lab. C. R. Mecanique 330, 185–191.
Duran, O., Parteli, E.J.R., Herrmann, H.J., 2010. A continuous model for sand dunes: review, new developments and application to barchans dunes and barchan dune fields. Earth Surf. Proc. Land. 35, 1591–1600.
Ewing, R.C., Hayes, A.G., Lucas, A., 2015. Sand dune patterns on Titan controlled by long-term climate cycles. Nat. Geosci. 8, 15–19.
Faria, R., Ferreira, A.D., Sismeiro, J.L., Mendes, J.C.F., Sousa, A.C.M., 2011. Wind tunnel and computational study of the stoss slope effect on the aeolian erosion of transverse sand dunes. Aeolian Res. 3, 303–314.
Franklin, E.M., Charru, F., 2011. Subaqueous barchan dunes in turbulent shear flow. Part1 Dune motion. J. Fluid Mech. 675, 199–222.
Gao, X., Zhang, D., Rozier, O., Narteau, C., 2014. Transport capacity and saturation mechanism in a real-space cellular automaton dune model. Adv. Geosci. 37, 47–55.
Groh, C., Wierschem, A., Aksel, N., Rehberg, I., Kruelle, C.A., 2008. Barchan dunes in two dimensions: experimental tests for minimal models. Phys. Rev. E 78, 021304.
Hersen, P., Douady, S., Andreotti, B., 2002. Relevant length scale of barchan dunes. Phys. Rev. Lett. 89, 264301.
Hersen, P., 2005. Flow effects on the morphology and dynamics of aeolian and subaqueous barchan dunes. J. Geophys. Res. 110, F04S07.
Hersen, P., 2004. On the crescentic shape of barchan dunes. Eur. Phys. J. B 37, 507–514.
Iversen, J.D., Rasmussen, K.R., 1994. The effect of surface slope on saltation threshold. Sedimentology 41, 721–728.
Katsuki, A., Nishimori, H., Endo, N., Taniguchi, K., 2005. Collision dynamics of two barchan dunes simulated by a simple model. J. Phys. Soc. Jpn. 74, 538–541.
Kok, J.F., Parteli, E.J.R., Michaels, T.I., Karam, D.B., 2012. The physics of wind-blown sand and dust. Rep. Prog. Phys. 75, 106901.
Koutsourakis, N., Venetsanos, A.G., Bartzis, J.G., 2012. LES modelling of hydrogen release and accumulation within a non-ventilated ambient pressure garage using the ADREA-HF CFD code. Int. J. Hydrogen Energy 37, 17426–17435.
Kroy, K., Sauermann, G., Herrmann, H.J., 2002. Minimal model for aeolian sand dunes. Phys. Rev. E 66, 031302.
Lima, A.R., Sauermann, G., Herrmann, H.J., Kroy, K., 2002. Modeling a dune field. Phys. A 310, 487–500.
Li, Z.Y., Tao, W.Q., 2002. A new stability-guaranteed second-order difference scheme. Numer. Heat Transfer B Fund. 42, 349–365.
Narteau, C., Zhang, D., Rozler, O., Claudin, P., 2009. Setting the length and time scales of a cellular automaton dune model from the analysis of superimposed bed forms. J. Geophys. Res. 114, F03006.
Ortiz, P., Smolarkiewicz, P.K., 2006. Numerical simulation of sand dune evolution in severe winds. Int. J. Numer. Methods Fluids 50, 1229–1246.
Pahtz, T., Parteli, E.J.R., Kok, J.F., Herrmann, H.J., 2014. Analytical model for flux saturation in sediment transport. Phys. Rev. E 89, 052213.
Parteli, E.J.R., Herrmann, H.J., 2003. A simple model for a transverse dune field. Phys. A 327, 554–562.
Parteli, E.J.R., Duran, O., Herrmann, H.J., 2007. Minimal size of a barchan dune. Phys. Rev. E 75, 011301.
Parteli, E.J.R., Duran, O., Bourke, M.C., Tsoar, H., Poschel, T., Herrmann, H.J., 2014a. Origins of barchan dune asymmetry: insights from numerical simulations. Aeolian Res. 12, 121–133.
Parteli, E.J.R., Kroy, K., Tsoar, H., Andrade Jr., J.S., Poschel, T., 2014b. Morphodynamic modeling of aeolian dunes: review and future plans. Eur. Phys. J. Special Topics 223, 2269–2283.
Patankar, S.V., 1980. Numerical Heat Transfer and Fluid Flow. Hemisphere, New York.
Pye, K., Tsoar, H., 2009. Aeolian Sand and Sand Dunes. Springer, Berlin.
Sauermann, G., Andrade Jr., J.S., Maia, L.P., Costa, U.M.S., Araujo, A.D., Herrmann, H.J., 2003. Wind velocity and sand transport on a barchan dune. Geomorphology 54, 245–255.
Sauermann, G., Kroy, K., Herrmann, H.J., 2001a. Continuum saltation model for sand dunes. Phys. Rev. E 64, 031305.
Sauermann, G., Kroy, K., Herrmann, H.J., 2001b. Saturation transients in saltation and their implications on dunes shapes. Phys. A 302, 244–254.
Schwammle, V., Herrmann, H.J., 2005. A model of barchan dunes including lateral shear stress. Eur. Phys. J. E 16, 57–65.
Schwammle, V., Herrmann, H.J., 2004. Modeling transverse dunes. Earth Surf. Proc. Land. 29, 769–784.
Smagorinsky, J., 1963. General circulation experiments with the primitive equations. I The basic experiment. Mon. Weather Rev. 91, 99–164.
Sorensen, M., 1991. An analytic model of wind-blown sand transport. Acta Mech. Suppl. 1, 67–81.
Wang, Z.T., Zheng, X.J., 2004. Theoretical prediction of creep flux in aeolian sand transport. Powder Technol. 139, 123–128.
Wedi, N.P., Smolarkiewicz, P.K., 2003. Extending Gal-Chen and Somerville terrain-following coordinate transformation on time-dependent curvilinear boundaries. J. Comput. Phys. 193, 1–20.
Werner, B.T., 1995. Eolian dunes: computer simulations and attractor interpretation. Geology 23, 1107–1110.
Werner, H., Wengle, H., 1991. Large-eddy simulation of turbulent flow over and around a cube in a plate channel. In: 8th Symposium on Turbulent Shear Flows, Munich, Germany, pp. 155–168.
Zhang, Y., Wang, Y., Jia, P., 2014. Evolution of downsized crescent-shaped dune in wind tunnel experiment. Sci. China G 57, 143–151.
Zheng, X.J., Bo, T.L., Zhu, W., 2009. A scale-coupled method for simulation of the formation and evolution of aeolian dune field. Int. J. Nonlinear Sci. Numer. 10, 387–395.